Study of nonstrange quark stars within a modified NJL model

Cheng-Ming Li,[1,*] Shu-Yu Zuo,[2] Ya-Peng Zhao,[3,†] Hui-Jun Mu,[1] and Yong-Feng Huang[4,‡]

[1]*School of Physics and Microelectronics, Zhengzhou University, Zhengzhou 450001, China*
[2]*College of Science, Henan University of Technology, Zhengzhou 450000, China*
[3]*School of Mathematics and Physics, Henan University of Urban Construction, Pingdingshan 467036, China*
[4]*School of Astronomy and Space Science, Nanjing University, Nanjing 210023, China*

(Received 15 July 2022; revised 29 October 2022; accepted 11 November 2022; published 14 December 2022)

In this work, a modified Nambu-Jona-Lasinio (NJL) model with proper-time regularization is employed to study the properties of hypothetical nonstrange quark stars. The coupling constant of the four-fermion interaction in the conventional NJL model is modified as $G = G_1 + G_2\langle\bar{\psi}\psi\rangle$ to highlight the feedback of the quark propagator to the gluon propagator. To study the dependence of the equation of state (EOS) on this modification as well as the vacuum pressure, we choose nine representative EOSs for comparison. It is found that a smaller G_1 leads to a stiffer EOS, and a higher vacuum pressure (i.e., a smaller bag constant) yields a softer EOS at low energy density. It is further shown that the heaviest quark star under this modified NJL model satisfies not only the recent mass measurement of PSR J0740 + 6620, but also the radius constraints from x-ray timing observations. The corresponding tidal deformability is also in agreement with the observations of GW170817.

DOI: 10.1103/PhysRevD.106.116009

I. INTRODUCTION

The structure of neutron stars and quark stars is largely determined by the equation of state (EOS) of dense matter. Given a particular EOS, the corresponding mass-radius ($M - R$) and mass-central energy density ($M - \epsilon_c$) relations can be obtained by solving the Tolman-Oppenheimer-Volkoff (TOV) equation. Since neutron stars and quark stars are composed of strongly interacting matter at high densities under a relatively low temperature, nonperturbative quantum chromodynamics (QCD) is deeply involved in exploring the EOS and structure of these compact stars. There are two critical features in QCD, i.e., color confinement and dynamical chiral symmetry breaking. At low chemical potentials, quarks are confined in hadrons under a low temperature. However, at high chemical potentials, quarks become deconfined. As a result, the observed highly compact pulsars could be quark stars rather than normal neutron stars.

In light of the hypothesis that strange quark matter might be the ground state of strongly interacting matter [1–4], many authors have extensively studied the characteristics of strange quark stars, either pure quark stars or hybrid neutron stars with a quark core [5–12]. Interestingly, a recent study [13] shows that stable quark matter might not be strange so that nonstrange quark stars can exist. Further studies have been carried out based on this viewpoint [14–18]. In Refs. [14,15], a new self-consistent mean-field approximation is employed to study the properties of nonstrange quark stars, such as the $M - R$ relation and the tidal deformability. Note that the difference between Ref. [14] and Ref. [15] is that the authors of Ref. [14] adopted the proper-time regularization, while a three-momentum cutoff regularization is used in Ref. [15]. A recent study [19] demonstrated that both the nonstrange and strange quark matter could be absolutely stable under the combination of the quark vector interaction and exchange interaction. Therefore, for two-flavor quark matter and three-flavor quark matter, which one is more stable is still an open question at present. In this study, we will investigate the properties of nonstrange quark stars in depth, providing useful constraints to the EOS of nonstrange quark matter with recent astronomical observations.

Since Joycelyn Bell and Antony Hewish discovered PSR B1919 + 21 in 1967, a large number of pulsar mass measurements have been obtained till now. Among these measurements, PSR J0348 + 0432 and PSR J0740 + 6620 are two special examples characterized by their large masses, i.e., $2.01 \pm 0.04\ M_\odot$ (solar mass) [20] and $2.14^{+0.10}_{-0.09}\ M_\odot$ [21], respectively. In recent years, the radii of a few pulsars were also measured at unprecedented

*licm@zzu.edu.cn
†zhaoyapeng2013@hotmail.com
‡hyf@nju.edu.cn

precision using data acquired by the Neutron Star Interior Composition Explorer (NICER) [22–24]. For example, in Ref. [22], the radius of a typical 1.44 $M_\odot$ pulsar is found to be larger than 10.7 km. Additionally, the recently discovered gravitational wave (GW) event GW170817 has opened a new era of multimessenger astronomy [25–40], and the LIGO-VIRGO collaboration provided useful constraints on the dimensionless tidal deformability (Λ) of neutron stars through GW waveform observations during the inspiral phase of the binary neutron star (BNS) merger. For the star of low-spin priors, it is estimated as $\Lambda(1.4\ M_\odot) \leq 800$ [25], and the $\Lambda_1 - \Lambda_2$ relation of GW170817 is also constrained by considering particular waveform models, such as the TaylorF2 waveform [41].

Lattice regularized QCD calculations are troubled by the famous "sign problem" at finite chemical potentials, making it difficult to perform calculations based on the first principles. As a result, we have to resort to some effective models to calculate the EOS of quark matter. Astronomical observations can then be used to test these hypothetical EOSs. In general, the EOS should not be too soft since it will fail to produce the massive stars of $\sim 2\ M_\odot$ as observed. At the same time, the EOS also should not be too stiff when the upper limit of the tidal deformability is considered, as hinted by the observational results of GW170817.

In this work we apply a modified Nambu-Jona-Lasinio (NJL) model to the case study of nonstrange quark stars. Inspired by the operator product expansion (OPE) approach, the traditional constant coupling coefficient of the 2-flavor NJL model is modified as $G = G_1 + G_2\langle\bar{\psi}\psi\rangle$ with $G_2\langle\bar{\psi}\psi\rangle$ accounting for the feedback of the quark propagator to the gluon propagator (see for instance Refs. [7,42–48]). The EOS of nonstrange quark matter derived in this framework will be used to study the properties of quark stars, especially the $M - R$ relation and the tidal deformability.

Many studies have focused on the NJL model with 't Hooft interaction [6,19]. Although our gap equation in the SU(2) case looks similar to previous SU(3) studies which possesses a quadratic dependence on the quark condensate, we would like to point out that the reason is different here. In Refs. [6,19], the t' Hooft interaction term leads to the above quadratic dependence. But in this study, the modification of the coupling constant G is responsible for the effect.

This paper is organized as follows. In Sec. II, a brief introduction on the modified 2-flavor NJL model is presented, and nine representative EOSs for nonstrange quark matter are introduced. In Sec. III, the tidal deformability and the $M - R$, $M - \epsilon_c$ relations are calculated for quark stars, and compared with astronomical observations. Finally, a brief summary and discussion is presented in Sec. IV.

II. EOS OF NONSTRANGE QUARK MATTER

The NJL model is widely used as an effective model to describe cold dense quark matter in neutron stars and quark stars [49,50]. The general form of the Lagrangian for the 2-flavor NJL model is

$$\mathcal{L} = \bar{\psi}(i\partial\!\!\!/ - m)\psi + G[(\bar{\psi}\psi)^2 + (\bar{\psi}i\gamma^5\tau\psi)^2], \tag{1}$$

where m denotes the current quark mass, and G is the four-fermion coupling constant.[1] The interaction term $G[(\bar{\psi}\psi)^2 + (\bar{\psi}i\gamma^5\tau\psi)^2]$ includes the scalar-isoscalar and pseudoscalar-isovector channels.

In general, the effective quark mass $m_{\rm eff}$ can be obtained by the self-consistent gap equation of

$$m_{\rm eff} = m - 2G\langle\bar{\psi}\psi\rangle, \tag{2}$$

where $\langle\bar{\psi}\psi\rangle$ is the quark condensate. At a zero temperature and zero chemical potential, it can be calculated as

$$\begin{aligned}\langle\bar{\psi}\psi\rangle &= -\int \frac{\mathrm{d}^4p}{(2\pi)^4}\mathrm{Tr}[iS(p^2)] \\ &= -N_c\int_{-\infty}^{+\infty}\frac{\mathrm{d}^4p}{(2\pi)^4}\frac{8im_{\rm eff}}{p^2 - m_{\rm eff}^2},\end{aligned} \tag{3}$$

where the trace "Tr" is evaluated in color, flavor, and Dirac spaces, and $S(p^2) = \frac{1}{\not{p} - m_{\rm eff}}$ represents the quark propagator.

To proceed, we need to convert our equations from the Minkowski space to the Euclidean space and employ some kinds of regularization. In this study, we adopt the proper-time regularization (PTR), a covariant regularization that has a "soft" cutoff to avoid the ultraviolet divergence when the momentum integration is to infinity. The formula of PTR is

$$\begin{aligned}\frac{1}{X^n} &= \frac{1}{(n-1)!}\int_0^\infty \mathrm{d}\tau\tau^{n-1}e^{-\tau X} \\ &\xrightarrow{\text{UV cutoff}} \frac{1}{(n-1)!}\int_{\tau_{\rm UV}}^\infty \mathrm{d}\tau\tau^{n-1}e^{-\tau X},\end{aligned} \tag{4}$$

where the integral limit $\tau_{\rm UV}$ is related to the ultraviolet cutoff $\Lambda_{\rm UV}$: $\tau_{\rm UV} = \Lambda_{\rm UV}^{-2}$. Adopting the PTR regularization, Eq. (3) becomes

[1] An exact isospin symmetry between u and d quark is adopted in this work so that $m_u = m_d = m$.

$$\begin{aligned}\langle\bar{\psi}\psi\rangle &= -N_c\int_{-\infty}^{+\infty}\frac{d^4p^E}{(2\pi)^4}\frac{8im_{\rm eff}}{(p^E)^2+m_{\rm eff}^2}\\ &= -\frac{N_c}{(2\pi)^4}\int_{-\infty}^{+\infty}\int_{-\infty}^{+\infty}d^3\vec{p}dp_4\frac{8m_{\rm eff}}{p_4^2+\vec{p}^2+m_{\rm eff}^2}\\ &= -\frac{6m_{\rm eff}}{\pi^2}\int_0^{+\infty}dp\frac{p^2}{\sqrt{p^2+m_{\rm eff}^2}}\\ &= -\frac{6m_{\rm eff}}{\pi^{\frac{2}{5}}}\int_{\tau_{\rm UV}}^{\infty}\int_0^{+\infty}d\tau dp\tau^{-\frac{1}{2}}p^2e^{-\tau(m_{\rm eff}^2+p^2)}\\ &= -\frac{6m_{\rm eff}}{4\pi^2}\int_{\tau_{\rm UV}}^{\infty}d\tau\frac{e^{-\tau m_{\rm eff}^2}}{\tau^2},\end{aligned}\tag{5}$$

where the superscript E means the parameter is measured in the Euclidean space.

The coupling constant G from the NJL model can be seen, under our current understanding of strong interactions, as a representation of an effective gluon propagator. Note that the quark and gluon propagators satisfy different Dyson-Schwinger (DS) equations, but they should couple with each other in view of QCD theory. As we know, quark propagators in the Nambu phase and Wigner phase are very different from each other [51–53], so the corresponding gluon propagators in these two phases should also be different. However, in the normal NJL model, G is simplified as a constant and remains the same in both the Nambu and the Wigner phases. Additionally, simulations of lattice QCD have shown that the gluon propagator should vary with temperature, while its dependence on the chemical potential is more uncertain. In most NJL calculations, the effective gluon propagator G is usually assumed to be "static," which thus does not depend on the temperature and chemical potential. This can be argued to be in contradiction with the requirements exerted on an effective gluon propagator.

The plane wave method in the QCD sum rule approach is used in Ref. [54]. It is argued that the full Green's function (which is unknown) can be divided into two parts: the nonperturbative part and the perturbative part. The condensates are then expressed as various moments of the nonperturbative Green's function. Therefore, the most general form of the "nonperturbative" gluon propagator is

$$D_{\mu\nu}^{\rm npert}\equiv D_{\mu\nu}^{\rm full}-D_{\mu\nu}^{\rm pert}\equiv c_1\langle\bar{\psi}\psi\rangle+c_2\langle G^{\mu\nu}G_{\mu\nu}\rangle+\cdots,\tag{6}$$

where $\langle G^{\mu\nu}G_{\mu\nu}\rangle$ is the gluon condensate, c_1 and c_2 are coefficients that can be calculated with the QCD sum rule approach [55,56], and the ellipsis refers to the contributions from other condensates (e.g., the mixed quark-gluon condensate).

Among all the condensates, the quark condensate has the lowest dimension, and a nonzero value of this quantity, in the chiral limit, just signals the dynamical chiral symmetry breaking. Therefore, it is the elementary item and plays the most important role in the QCD sum rule approach. In this study, we will treat its contribution separately, while the contribution of other condensates is included in the perturbative part of the gluon propagator. In the framework of the NJL model, it is equivalent to a modification of

$$G\to G_1+G_2\langle\bar{\psi}\psi\rangle,\tag{7}$$

which is quite similar to the approach in Refs. [7,42–48]. Under this modification, the coupling strength G will depend on both u and d quark condensates. G_2 can be regarded as an effective coupling strength, reflecting the relative weight of the influence of the quark propagator and gluon propagator.[2]

TABLE I. Parameters adopted in this study.

m [MeV]	$\Lambda_{\rm UV}$ [MeV]	$m_{\rm eff}$ [MeV]	$-\langle\bar{\psi}\psi\rangle^{\frac{1}{3}}$ [MeV]	G [GeV^{-2}]	G_1 [GeV^{-2}]	G_2 [GeV^{-5}]
3.5	1324	180	353	2.005	1.935	−1.582
					2.005	0
					2.100	2.161

In this study, we will take three representative sets of (G_1, G_2) and then constrain the corresponding EOSs with astronomical observations (see Sec. III for more details). The current quark mass is taken as $m=(m_u+m_d)/2=3.5$ MeV [57]. Similar to Ref. [49], we fix the parameters $(\Lambda_{\rm UV}, G)$ to reproduce the experimental data ($f_\pi=92$ MeV, $m_\pi=135$ MeV). The complete parameter sets adopted, including G_1 and G_2, are presented in Table I.

Here, we will also extend our calculations to zero temperature and finite chemical potential, which is equivalent to performing a transformation in the Euclidean space as [58]

$$p_4\to p_4+i\mu.\tag{8}$$

The quark condensate and number density, in the vanishing temperature case, can then be derived as

$$\begin{aligned}\langle\bar{\psi}\psi\rangle &= -N_c\int_{-\infty}^{+\infty}\frac{d^4p}{(2\pi)^4}\frac{8m_{\rm eff}}{(p_4+i\mu)^2+m_{\rm eff}^2+\vec{p}^2}\\ &= -\frac{6m_{\rm eff}}{\pi^3}\int_0^{+\infty}dp\int_{-\infty}^{+\infty}dp_4\frac{p^2}{(p_4+i\mu)^2+m_{\rm eff}^2+p^2}\\ &= \begin{cases}-\frac{6m_{\rm eff}}{\pi^2}\int_{\sqrt{\mu^2-m_{\rm eff}^2}}^{+\infty}dp\frac{[1-{\rm Erf}(\sqrt{m_{\rm eff}^2+p^2}\sqrt{\tau_{\rm UV}})]p^2}{\sqrt{m_{\rm eff}^2+p^2}}, & m_{\rm eff}<\mu\\ \frac{3m_{\rm eff}}{2\pi^2}[-m_{\rm eff}^2{\rm Ei}(-m_{\rm eff}^2\tau_{\rm UV})-\frac{e^{-m_{\rm eff}^2\tau_{\rm UV}}}{\tau_{\rm UV}}], & m_{\rm eff}>\mu\end{cases}\end{aligned}\tag{9}$$

[2]In a conventional two-flavor NJL model, the thermodynamical potential is obtained based on the mean-field approximation, see, e.g., Eq. (2.46) in Ref. [50] (neglecting the contribution of the vector interaction). The modification here can be regarded as a scheme beyond the mean-field approach, and it is hard to find a closed and easily tractable effective potential (a more detailed analysis can be found in Sec. 2 of Ref. [43]).

$$\begin{aligned}\rho_{\mathrm{i}}(\mu) &= \langle\psi^{+}\psi\rangle_{\mathrm{i}} \\ &= -N_{\mathrm{c}}\int\frac{\mathrm{d}^4p}{(2\pi)^4}tr[iS_{\mathrm{i}}\gamma_0] \\ &= 2N_{\mathrm{c}}\int\frac{\mathrm{d}^3p}{(2\pi)^3}\theta(\mu-\sqrt{p^2+m_{\mathrm{eff}}^2}) \\ &= \begin{cases}\frac{1}{\pi^2}(\sqrt{\mu^2-m_{\mathrm{eff}}^2})^3, & \mu > m_{\mathrm{eff}} \\ 0, & \mu < m_{\mathrm{eff}}\end{cases} \end{aligned} \tag{10}$$

where the subscript "i" denotes the quark of flavor i, and the trace "tr" is calculated in the Dirac space. The effective quark mass m_{eff} as a function of the chemical potential at zero temperature is shown in Fig. 1. The number density $\rho_{\mathrm{u,d}}$ is correspondingly illustrated in Fig. 2.

In the framework of the NJL model, many researchers [50,59,60] have demonstrated that whether there is a first order chiral phase transition at zero temperature (when $m_{\mathrm{u}} \neq 0$) depends on the regularization being employed, even though the modification $G \to G_1 + G_2\langle\bar{\psi}\psi\rangle$ was not adopted in their studies. In Ref. [50], three dimensional (3D) momentum cutoff regularization was used and a first order phase transition was reported to happen at $T = 0$. However, in Ref. [59], the authors used the PTR and only got a crossover transition at $T = 0$. In particular, Ref. [60] studied the effects of regularization on the phase diagram by using the NJL model. In the case of low current quark mass, such as $m_{\mathrm{u}} = 3$ MeV, only a crossover could be observed at $T = 0$ for both PTR and 3D regularization.

In this study, the PTR is also used for the case of low current quark mass ($m_{\mathrm{u}} = 3.5$ MeV). The parameter set with $G_1 = 2.005$ GeV^{-2} just corresponds to the normal 2-flavor NJL model. Figure 1 shows that when the chemical potential increases from 0 to 700 MeV, we could only observe a crossover for the parameter sets in Table I, but not the first order phase transition.

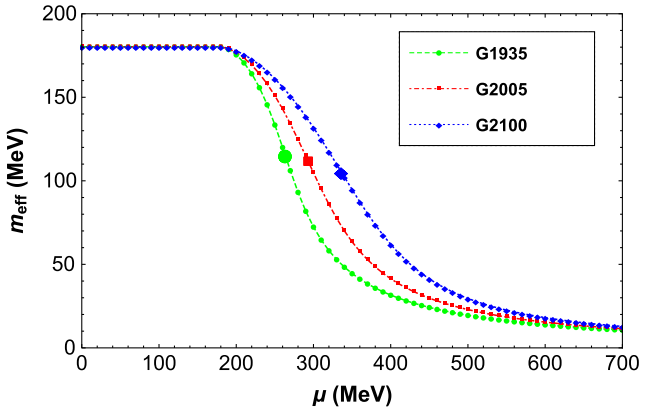

FIG. 1. The effective quark mass versus μ at $T = 0$. The lines marked with G1935, G2005, and G2100 correspond to the three parameter sets in Table I, with $G_1 = 1.935, 2.005, 2.100$ GeV^{-2}, respectively. The pseudocritical point is also marked on each line, at $\mu = 263, 293, 336$ MeV, respectively.

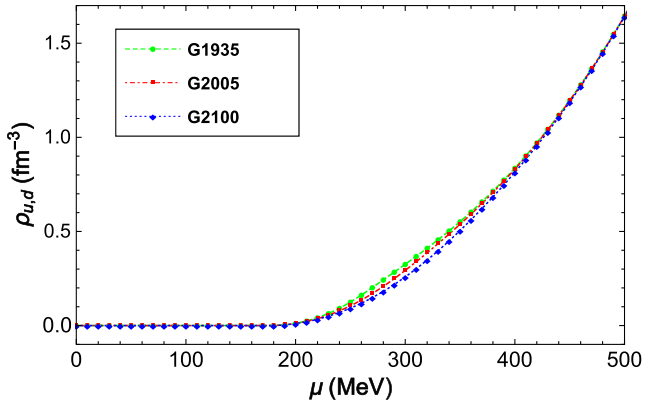

FIG. 2. The number density of u, d quarks versus μ at $T = 0$ for the three parameter sets in Table I. Line styles are the same as those in Fig. 1.

In fact, we have also varied the value of G_1 between 1.0 and 3.0 GeV^{-2} to study the properties of the phase transition at $T = 0$. When $G_1 < 1.8$ GeV^{-2}, a first order phase transition happens, and the critical chemical potential is $\mu_{\mathrm{c}} = 180$ MeV. However, when $G_1 > 1.8$ GeV^{-2}, a crossover would be obtained, and the pseudocritical chemical potential increases together with G_1. Different from the meaning of the so-called "critical chemical potential" in the first order phase transition, the "pseudocritical chemical potential" here refers to the crossover condition, corresponding to the inflection point in the curves of condensate and the effective quark mass.

Here we present some further explanations on how the three representative values are chosen for G_1 in Table I. In Sec. III, we could see that all the EOSs with $B^{1/4} = 115$ MeV can support massive nonstrange quark stars of two solar mass. However, a too large or too small value of G_1 can make the EOS conflict with the tidal deformability measurement of GW170817. To roughly meet this requirement, we finally take the parameter as $G_1 = 1.935$, 2.005 (the normal NJL model), and 2.100 GeV^{-2} in this study.

Note that the chemical potential of the pseudocritical point is different for the three lines in Fig. 1, as marked in Fig. 1. It can also be seen that at zero temperature and zero chemical potential, the effective quark masses are the same for the three parameter sets. This is easy to understand. Under such a condition, $G_1 + G_2\langle\bar{\psi}\psi\rangle$ simply reduces to G, which is exactly the coupling constant of conventional NJL model. In Fig. 2, we see that the quark densities differ only in the crossover region of $\mu \sim (200, 400)$ MeV for the three parameter sets.

Considering the electrical neutrality of neutron stars and quark stars as well as electroweak reactions in them, we should take the beta equilibrium and electric charge neutrality conditions into account,

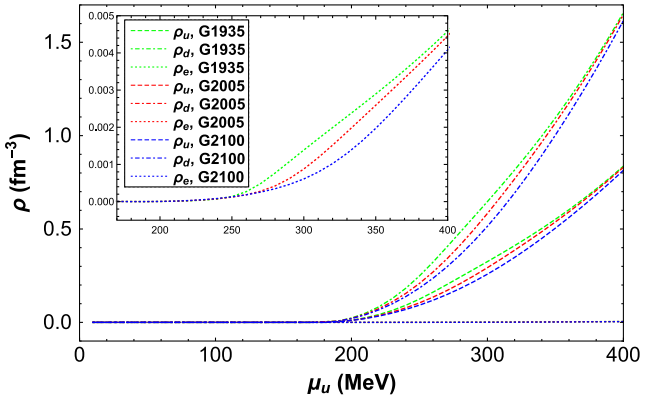

FIG. 3. The number densities of u, d quarks and electrons versus μ_{u} at $T = 0$. The matter here is in beta equilibrium and electric charge neutrality. The parameter sets are described in Table I. The inset shows a zoom-in of the electron densities.

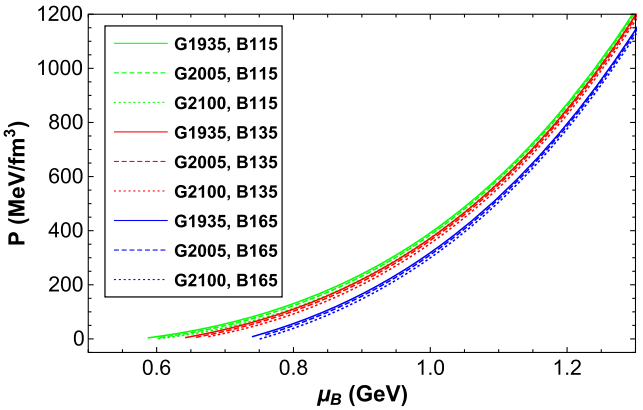

FIG. 4. The pressure as a function of the baryonic chemical potential (μ_{B}) for nine representative EOSs at $T = 0$. B115, B135, B165 refers to $B^{\frac{1}{4}} = 115$, 135, 165 MeV, respectively.

$$\mu_{\mathrm{d}} = \mu_{\mathrm{u}} + \mu_{\mathrm{e}},$$
$$\frac{2}{3}\rho_{\mathrm{u}} - \frac{1}{3}\rho_{\mathrm{d}} - \rho_{\mathrm{e}} = 0, \tag{11}$$

where the number density of electrons at zero temperature is $\rho_{\mathrm{e}}(\mu_{\mathrm{e}}) = \frac{\mu_{\mathrm{e}}^3}{3\pi^2}$. The number densities of quarks and electrons incorporating these conditions are displayed in Fig. 3. We can see that in each case, the density of d quarks is larger than that of u quarks when $\mu_{\mathrm{u}} > 180$ MeV. In fact ρ_{d} approximately equals $2\rho_{\mathrm{u}}$, because the electron density is much smaller. Figure 3 also shows that as G_1 increases, the constituent particle number density decreases for the same μ_{u} when $\mu_{\mathrm{u}} \geq 180$ MeV. This is expected as it is the value for the dynamical mass of the quarks in the vacuum and therefore the chemical potential at which we see changes in the system at zero temperature.

It is well known that under the beta equilibrium and electric charge neutrality conditions, the quark condensates, dynamical masses, and densities are different for u quarks and d quarks. But note that these quantities are connected with each other, and the relations between them should be considered when calculating the EOS.

By definition, the EOS of QCD for $T = 0$ and $\mu \neq 0$ is [61]

$$P(\mu) = P(\mu = 0) + \int_0^{\mu} \mathrm{d}\mu' \rho(\mu'), \tag{12}$$

where $P(\mu = 0)$ represents the negative vacuum pressure and is independent on the chemical potential. In general, it is treated as a phenomenological parameter which cannot be calculated model-independently. The parameter of $P(\mu = 0)$ in QCD is equivalent to the vacuum bag constant $(-B)$ of the MIT bag model. Generally, $B^{\frac{1}{4}}$ should be in a range of 100–200 MeV [62,63]. More specifically, in Ref. [33] and Ref. [64], it is suggested to be 134.1–141.4 MeV and 166.16–171.06 MeV, respectively. Therefore, in this study, we will choose three representative values of $B^{\frac{1}{4}}$ to calculate the nonstrange quark EOS, i.e., $B^{\frac{1}{4}} = 115$, 135, 165 MeV. Note that the parameter $B^{\frac{1}{4}}$ has to be fixed when calculating the EOS, and it does not affect the gap equation as well as the $m_{\mathrm{eff}} - \mu$ relation in the former step.

The results of nine representative EOSs are illustrated in Fig. 4. We see that the pseudocritical baryonic chemical potential μ_{BC},[3] referring to the condition that the pressure begins to be nonzero with "pseudo" related to the crossover, increases as $B^{\frac{1}{4}}$ or G_1 increases. Additionally, we see that the EOS is largely determined by the bag constant, while the parameter of G_1 does not affect the EOS significantly.

The relation between the energy density and pressure is [65,66]

$$\epsilon = -P + \sum_i \mu_{\mathrm{i}} \rho_{\mathrm{i}}. \tag{13}$$

To illustrate the rationality of the nine quark EOSs as well as their stiffness, we calculate the sound velocity, which is

$$\nu = \sqrt{\frac{\mathrm{d}P}{\mathrm{d}\epsilon}}. \tag{14}$$

The results are shown in Fig. 5. We see that the sound velocity does not exceed the conformal limit in all the cases, i.e., $(\nu/c)^2 \leq 1/3$, where c is the speed of light. Usually, a smaller G_1 leads to a stiffer EOS. Also, note that at low energy densities, a higher vacuum pressure (i.e., a smaller $B^{\frac{1}{4}}$) yields a softer EOS, but at high energy densities, the case is opposite.

[3]For 2-flavor quark matter, the baryonic chemical potential is $\mu_{\mathrm{B}} = \mu_{\mathrm{u}} + \mu_{\mathrm{d}}$.

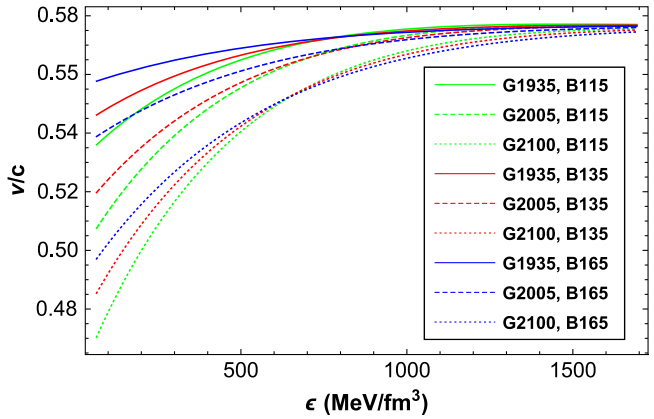

FIG. 5. The sound velocity versus energy density for the nine representative EOSs. Line styles are the same as in Fig. 4.

III. STRUCTURE OF NONSTRANGE QUARK STARS

To study the structure of neutron stars and quark stars, we need to solve the TOV equation below,

$$\frac{\mathrm{d}P(r)}{\mathrm{d}r} = -\frac{G(\epsilon+P)(M+4\pi r^3 P)}{r(r-2GM)},$$
$$\frac{\mathrm{d}M(r)}{\mathrm{d}r} = 4\pi r^2 \epsilon. \tag{15}$$

Using the nine representative EOSs, we have solved the equation numerically. Our results of $M-R$ and $M-\epsilon_c$ relations are presented in Figs. 6 and 7, respectively. To constrain the EOSs, we have also plotted some astronomical measurements in Fig. 6, including the largest pulsar masses (i.e., $2.01 \pm 0.04\ M_\odot$ for PSR J0348 + 0432 [20], and $2.14^{+0.10}_{-0.09}\ M_\odot$ for PSR J0740 + 6620 [21]), and the radii measured through NICER x-ray timing observations

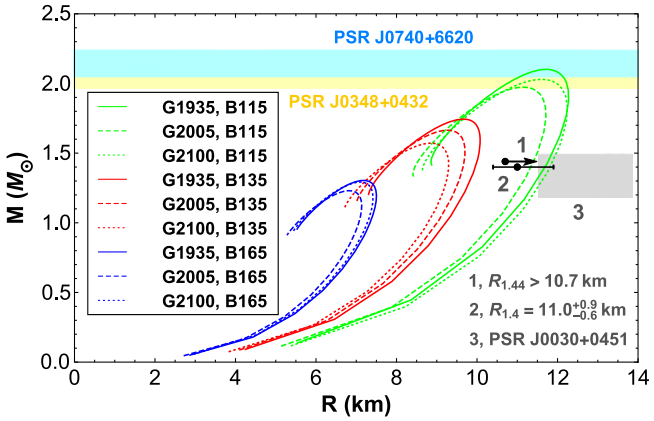

FIG. 6. $M-R$ relations for the nine representative EOSs. The mass constrains of PSR J0348 + 0432 [20] and PSR J0740 + 6620 [21], and the radius constraints from NICER x-ray timing observations [22–24] are also plotted.

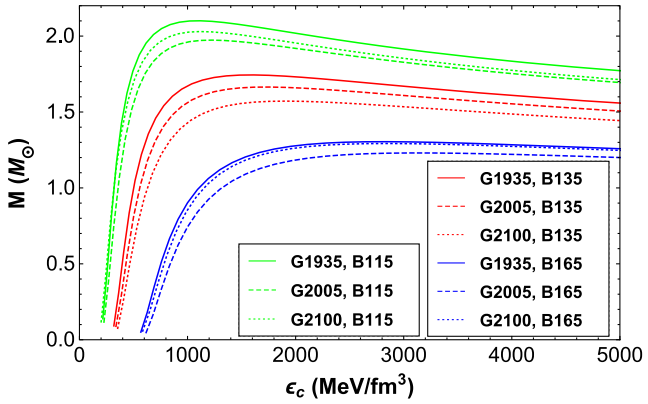

FIG. 7. $M-\epsilon_c$ relations for the nine representative EOSs.

(1, $R_{1.44\,M_\odot} > 10.7$ km [22]; 2, $R_{1.4\,M_\odot} = 11.0^{+0.9}_{-0.6}$ km [23]; 3, $M = 1.34^{+0.15}_{-0.16}\ M_\odot$ and $R = 12.71^{+1.14}_{-1.19}$ km for PSR J0030 + 0451 [24]). From Fig. 6, we see that only the EOS with $G_1 = 1.935\ \mathrm{GeV}^{-2}$ and $B^{\frac{1}{4}} = 115$ MeV satisfies all the above constraints, and the corresponding maximum mass of quark stars is $2.10\ M_\odot$, with a radius of 11.69 km. When G_1 is fixed, the EOS with a smaller bag constant produces a larger maximum star mass. In Fig. 7, a higher maximum mass generally corresponds to a smaller central energy density.

We have also calculated the tidal deformability of quark stars. To do so, we need to solve a set of differential equations [67],

$$\begin{aligned}\frac{\mathrm{d}H}{\mathrm{d}r} &= \beta,\\ \frac{\mathrm{d}\beta}{\mathrm{d}r} &= 2\left(1-2\frac{m_r}{r}\right)^{-1} H\left\{-2\pi[5\epsilon+9P+f(\epsilon+P)]\right.\\ &\quad \left.+\frac{3}{r^2}+2\left(1-2\frac{m_r}{r}\right)^{-1}\left(\frac{m_r}{r^2}+4\pi r P\right)^2\right\}\\ &\quad +\frac{2\beta}{r}\left(1-2\frac{m_r}{r}\right)^{-1}\left\{\frac{m_r}{r}+2\pi r^2(\epsilon-P)-1\right\},\end{aligned} \tag{16}$$

where P and $H(r)$ represent the pressure and the metric function, respectively, and $f = \mathrm{d}\epsilon/\mathrm{d}P$. Let us further define a parameter (y) as $y = R\beta(R)/H(R) - 4\pi R^3\epsilon_0/M$, where ϵ_0 is the energy density at the surface of the star. Then the dimensionless tidal Love number k_2 for $l = 2$ can be calculated as

$$\begin{aligned}k_2 &= \frac{8C^5}{5}(1-2C)^2[2+2C(y-1)-y]\\ &\quad \times\{2C[6-3y+3C(5y-8)]\\ &\quad +4C^3[13-11y+C(3y-2)+2C^2(1+y)]\\ &\quad +3(1-2C)^2[2+2C(y-1)-y]\ln(1-2C)\}^{-1},\end{aligned} \tag{17}$$

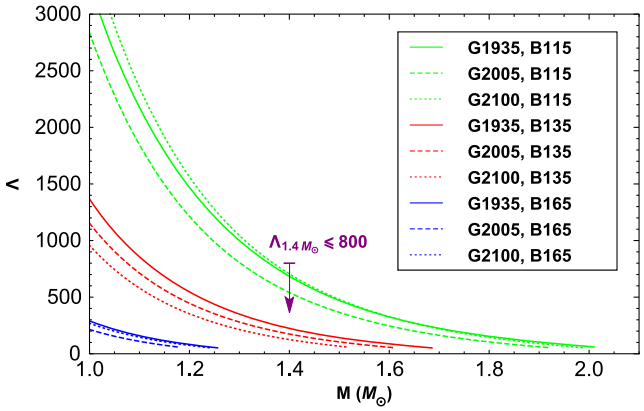

FIG. 8. Tidal deformability of nonstrange quark stars for the nine representative EOSs. The constraint of $\Lambda(1.4\ M_\odot) \leq 800$ from Ref. [25] is also plotted.

where $C = M/R$ is the compactness of the star. According to Ref. [67], the tidal deformability is related to k_2 as

$$\Lambda = \frac{2}{3} k_2 R^5. \tag{18}$$

Note that the quark matter in quark stars is in a deconfined state. It produces a positive pressure at the surface. Due to the negative vacuum pressure in Eq. (12), the surface quark density should be nonzero.

Our numerical results on the tidal deformability of nonstrange quark stars for the nine representative EOSs are shown in Fig. 8. We see that the tidal deformability decreases monotonically as the mass increases. EOSs with $B^{\frac{1}{4}} = 115$, 135 MeV satisfy the constraint of $\Lambda(1.4\ M_\odot) \leq 800$ derived from the observations of GW170817 for the low-spin priors [25]. Furthermore, based on the waveform model of TaylorF2, the chirp mass $\mathcal{M} = (M_1 M_2)^{3/5}(M_1 + M_2)^{-1/5}$ is restricted to be $1.186 \pm 0.0001\ M_\odot$, providing further constraint on companion mass of M_1 and M_2 for GW170817 [41]. Thus the $\Lambda_1 - \Lambda_2$ relation of the BNS can be obtained for our nine representative EOSs, which is shown in Fig. 9. Here, the constraint from GW170817 based on the TaylorF2 waveform model [41] is also plotted for a direct comparison. We see that every EOS with $M_{\max} \geq 1.36\ M_\odot$ (i.e., the EOSs with $B^{\frac{1}{4}} = 115$, 135 MeV) fulfills the constraint except for the EOS with $G_1 = 2.1\ \mathrm{GeV}^{-2}$ and $B^{\frac{1}{4}} = 115$ MeV. In addition to that, a larger $B^{\frac{1}{4}}$ makes the curve closer to the lower left corner of the figure.

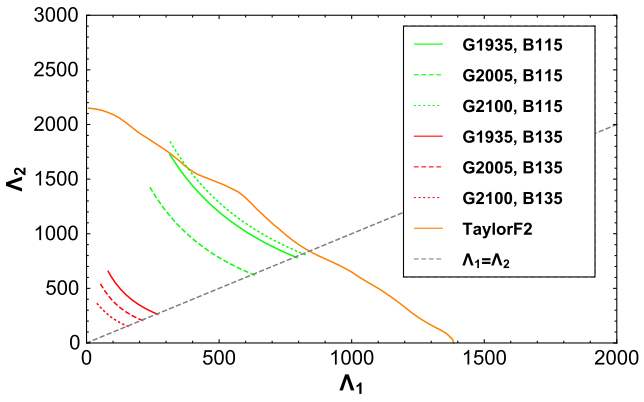

FIG. 9. $\Lambda_1 - \Lambda_2$ relations for the nine representative EOSs. The observational constraint from GW170817 based on the TaylorF2 waveform model is also plotted for comparison [41].

For the sake of completeness, the properties of nonstrange quark stars for the nine representative EOSs are summarized in Table II. The parameters listed include the mass, radius, surface and central energy densities of the heaviest star, and the tidal deformability and radius of a $1.4\ M_\odot/1.6\ M_\odot$ star. From Figs. 6, 9, and Table II, we can see that the parameter sets with $B^{\frac{1}{4}} = 115$ MeV support more massive stars, while the EOSs with $G_1 = 2.005\ \mathrm{GeV}^{-2}$ correspond to the original 2-flavor NJL model. Although the EOSs of the normal NJL model can satisfy the constraints of the tidal deformability from GW170817, they are not consistent with the mass constraint from PSR J0740 + 6620 and the radius constraint from PSR J0030 + 0451. In particular, for $B^{\frac{1}{4}} = 115$ MeV, both increasing and decreasing the value of G_1 can increase the maximum mass, but a too large or too small value of G_1 makes the EOS conflict with the tidal deformability measurement of GW170817. Among the nine representative EOSs, only the one with $B^{\frac{1}{4}} = 115$ MeV and $G_1 = 1.935\ \mathrm{GeV}^{-2}$ is in agreement with all current astronomical measurements considered in this study. Based on these analyses, we argue that nonstrange quark stars might exist in the universe.

IV. SUMMARY AND DISCUSSION

The EOS of a modified 2-flavor NJL model with PTR is introduced to investigate the properties of nonstrange quark stars. Since the coupling constant G in the normal NJL model is an indication of the effective gluon propagator, it should not be "constant" according to the simulation of lattice QCD. The corresponding DS equation should be coupled with that of quarks by QCD in essence. Inspired by the OPE method, the coupling constant G is modified as $G = G_1 + G_2\langle\bar{\psi}\psi\rangle$ in this study, similar to the treatment in Refs. [7,42–48]. The electric charge neutrality and beta equilibrium are considered in our calculations. Nine representative EOSs are obtained for nonstrange quark stars, corresponding to different combinations of G_1 and B (the bag constant) parameters. The pseudocritical point on the $P - \mu_B$ plane just refers to the surface of the quark star where the pressure becomes nonzero (the pressure inside the star is higher than that). A larger B (or G_1) leads to a larger surface baryonic chemical potential. To illustrate the stiffness and rationality of the EOSs, the sound velocity is calculated. It is found that the sound velocity is ubiquitously smaller than the speed of light, not exceeding the conformal limit for dense matter. It is also found that a smaller G_1

TABLE II. Properties of nonstrange quark stars for the nine representative EOSs.

$B^{\frac{1}{4}}$ [MeV]	G_1 [GeV^{-2}]	$M_{\max}$ [$M_\odot$]	R_m [km]	ϵ_0 [MeV/fm^3]	ϵ_c [MeV/fm^3]	$\Lambda(1.4)$ ···	$R(1.4)$ [km]	$\Lambda(1.6)$ ···	$R(1.6)$ [km]
	1.935	2.10	11.69	178	1118	679	11.70	324	12.01
115	2.005	1.97	11.14	188	1227	539	11.35	246	11.60
	2.100	2.03	11.62	166	1113	702	11.83	325	12.10
	1.935	1.74	9.63	277	1612	222	9.96	83	10.08
135	2.005	1.66	9.25	291	1756	176	9.65	59	9.64
	2.100	1.57	8.85	305	1909	124	9.31	···	···
	1.935	1.30	7.17	513	2848	···	···	···	···
165	2.005	1.23	6.84	555	3066	···	···	···	···
	2.100	1.29	7.09	521	2860	···	···	···	···

usually leads to a stiffer EOS. Interestingly, for the bag constant, a smaller B parameter yields a softer EOS at low densities; but at high densities, the case is opposite.

The $M-R$, $M-\epsilon_c$ relations and the tidal deformability of quark stars are calculated based on our new EOSs. The results are directly compared with recent astronomical observations, including the mass measurements of PSR J0740 + 6620 ($2.14^{+0.10}_{-0.09}$ $M_\odot$) [21] and PSR J0348 + 0432 (2.01 ± 0.04 $M_\odot$) [20], the radius measurements by NICER ($R_{1.44\ M_\odot} > 10.7$ km [22], $R_{1.4\ M_\odot} = 11.0^{+0.9}_{-0.6}$ km [23], $M = 1.34^{+0.15}_{-0.16}$ $M_\odot$ and $R = 12.71^{+1.14}_{-1.19}$ km for PSR J0030 + 0451 [24]), and the tidal deformability constraints from GW170817 [25,41]. It is found that when the two key parameters are taken as $G_1 = 1.935$ GeV^{-2} and $B^{\frac{1}{4}} = 115$ MeV, the corresponding EOS can satisfy all the observational constraints listed above, strongly supporting the possible existence of nonstrange quark stars. In this case, the nonstrange quark star can have a maximum mass of 2.1 $M_\odot$, with a radius of 11.69 km.

In the future, more and more astronomical measurements will be available, which can help better constraining the EOS of QCD. Note that only the relatively simple case of four-fermion interactions is considered here. But the method could also be extended to include more interactions, such as the 't Hooft and eight-quark interactions. To do that, we need to consider how to deal with their coupling consistently. For the normal SU(3) case, more free parameters (the current masses of u, d, s quarks, the coupling constants of four-, six-, eight-quark interactions, and the ultraviolet cutoff) would be introduced to characterize the six- and eight-quark interactions in the NJL model. They should be determined through various laboratory experiments and astronomical observations, and should be considered in future theoretical studies.

ACKNOWLEDGMENTS

We thank the anonymous referee for helpful comments and suggestions that led to an overall improvement of this study. This work is supported in part by the National Natural Science Foundation of China (under Grants No. 12005192, No. 12103047, No. 12233002, No. 11873030, No. 12041306, No. 12147103, and No. U1938201), the Project funded by China Postdoctoral Science Foundation (No. 2020M672255, No. 2020TQ0287), National SKA Program of China No. 2020SKA0120300, the National Key R&D Program of China (2021YFA0718500), the science research grants from the China Manned Space Project with No. CMS-CSST-2021-B11, the Natural Science Foundation of Henan Province of China (No. 212300410290), the start-up funding from Zhengzhou University, and the High-level Talent Fund of Henan University of Technology (Grant No. 31401242).

[1] N. Itoh, Prog. Theor. Phys. **44**, 291 (1970).
[2] H. Terazawa, J. Phys. Soc. Japan **58**, 1989 (1979).
[3] A. R. Bodmer, Phys. Rev. D **4**, 1601 (1971).
[4] E. Witten, Phys. Rev. D **30**, 272 (1984).
[5] E. Farhi and R. L. Jaffe, Phys. Rev. D **30**, 2379 (1984).
[6] C.-M. Li, J.-L. Zhang, T. Zhao, Y.-P. Zhao, and H.-S. Zong, Phys. Rev. D **95**, 056018 (2017).
[7] C.-M. Li, J.-L. Zhang, Y. Yan, Y.-F. Huang, and H.-S. Zong, Phys. Rev. D **97**, 103013 (2018).
[8] B.-L. Li, Z.-F. Cui, Z.-H. Yu, Y. Yan, S. An, and H.-S. Zong, Phys. Rev. D **99**, 043001 (2019).
[9] C.-M. Li, S.-Y. Zuo, Y. Yan, Y.-P. Zhao, F. Wang, Y.-F. Huang, and H.-S. Zong, Phys. Rev. D **101**, 063023 (2020).
[10] B.-L. Li, Y. Yan, and J.-L. Ping, Eur. Phys. J. C **81**, 1 (2021).

[11] J. Sedaghat, S. Zebarjad, G. Bordbar, and B. Eslam Panah, Phys. Lett. B **829**, 137032 (2022).
[12] J. Geng, B. Li, and Y. Huang, Innovation **2**, 100152 (2021).
[13] B. Holdom, J. Ren, and C. Zhang, Phys. Rev. Lett. **120**, 222001 (2018).
[14] Q. Wang, C. Shi, and H.-S. Zong, Phys. Rev. D **100**, 123003 (2019).
[15] T. Zhao, W. Zheng, F. Wang, C.-M. Li, Y. Yan, Y.-F. Huang, and H.-S. Zong, Phys. Rev. D **100**, 043018 (2019).
[16] C. Zhang, Phys. Rev. D **101**, 043003 (2020).
[17] J. Ren and C. Zhang, Phys. Rev. D **102**, 083003 (2020).
[18] C. Zhang and R. B. Mann, Phys. Rev. D **103**, 063018 (2021).
[19] W.-L. Yuan, A. Li, Z. Miao, B. Zuo, and Z. Bai, Phys. Rev. D **105**, 123004 (2022).
[20] J. Antoniadis *et al.*, Science **340**, 1233232 (2013).
[21] H. T. Cromartie, E. Fonseca, S. M. Ransom, P. B. Demorest, Z. Arzoumanian, H. Blumer, P. R. Brook, M. E. DeCesar, T. Dolch, J. A. Ellis *et al.*, Nat. Astron. **4**, 72 (2020).
[22] S. Bogdanov, S. Guillot, P. S. Ray, M. T. Wolff, D. Chakrabarty, W. C. Ho, M. Kerr, F. K. Lamb, A. Lommen, R. M. Ludlam *et al.*, Astrophys. J. Lett. **887**, L25 (2019).
[23] C. D. Capano, I. Tews, S. M. Brown, B. Margalit, S. De, S. Kumar, D. A. Brown, B. Krishnan, and S. Reddy, Nat. Astron. **4**, 625 (2020).
[24] T. E. Riley, A. L. Watts, S. Bogdanov, P. S. Ray, R. M. Ludlam, S. Guillot, Z. Arzoumanian, C. L. Baker, A. V. Bilous, D. Chakrabarty *et al.*, Astrophys. J. Lett. **887**, L21 (2019).
[25] B. P. Abbott *et al.* (LIGO Scientific and Virgo Collaborations), Phys. Rev. Lett. **119**, 161101 (2017).
[26] B. P. Abbott *et al.* (LIGO Scientific and Virgo Collaborations), Astrophys. J. Lett. **848**, L12 (2017).
[27] E. Annala, T. Gorda, A. Kurkela, and A. Vuorinen, Phys. Rev. Lett. **120**, 172703 (2018).
[28] F. J. Fattoyev, J. Piekarewicz, and C. J. Horowitz, Phys. Rev. Lett. **120**, 172702 (2018).
[29] B. Margalit and B. D. Metzger, Astrophys. J. Lett. **850**, L19 (2017).
[30] A. Bauswein, O. Just, H.-T. Janka, and N. Stergioulas, Astrophys. J. Lett. **850**, L34 (2017).
[31] V. Paschalidis, K. Yagi, D. Alvarez-Castillo, D. B. Blaschke, and A. Sedrakian, Phys. Rev. D **97**, 084038 (2018).
[32] M. Shibata, S. Fujibayashi, K. Hotokezaka, K. Kiuchi, K. Kyutoku, Y. Sekiguchi, and M. Tanaka, Phys. Rev. D **96**, 123012 (2017).
[33] E.-P. Zhou, X. Zhou, and A. Li, Phys. Rev. D **97**, 083015 (2018).
[34] M. Ruiz, S. L. Shapiro, and A. Tsokaros, Phys. Rev. D **97**, 021501(R) (2018).
[35] D. Radice, A. Perego, F. Zappa, and S. Bernuzzi, Astrophys. J. Lett. **852**, L29 (2018).
[36] L. Rezzolla, E. R. Most, and L. R. Weih, Astrophys. J. Lett. **852**, L25 (2018).
[37] R. Nandi and P. Char, Astrophys. J. **857**, 12 (2018).
[38] Z.-Y. Zhu, E.-P. Zhou, and A. Li, Astrophys. J. **862**, 98 (2018).
[39] S. Ai, H. Gao, Z.-G. Dai, X.-F. Wu, A. Li, B. Zhang, and M.-Z. Li, Astrophys. J. **860**, 57 (2018).
[40] Y.-L. Ma, H. K. Lee, W.-G. Paeng, and M. Rho, Sci. China Phys. Mech. Astron. **62**, 1 (2019).
[41] B. P. Abbott *et al.* (LIGO Scientific and Virgo Collaborations), Phys. Rev. X **9**, 011001 (2019).
[42] Y. Jiang, H. Gong, W.-M. Sun, and H.-S. Zong, Phys. Rev. D **85**, 034031 (2012).
[43] Z.-F. Cui, C. Shi, Y.-H. Xia, Y. Jiang, and H.-S. Zong, Eur. Phys. J. C **73**, 2612 (2013).
[44] Z.-F. Cui, C. Shi, W.-M. Sun, Y.-L. Wang, and H.-S. Zong, Eur. Phys. J. C **74**, 2782 (2014).
[45] C. Shi, Y.-L. Du, S.-S. Xu, X.-J. Liu, and H.-S. Zong, Phys. Rev. D **93**, 036006 (2016).
[46] Q.-W. Wang, Z.-F. Cui, and H.-S. Zong, Phys. Rev. D **94**, 096003 (2016).
[47] Z.-Y. Fan, W.-K. Fan, Q.-W. Wang, and H.-S. Zong, Mod. Phys. Lett. A **32**, 1750107 (2017).
[48] W. Fan, X. Luo, and H. Zong, Chin. Phys. C **43**, 054109 (2019).
[49] S. P. Klevansky, Rev. Mod. Phys. **64**, 649 (1992).
[50] M. Buballa, Phys. Rep. **407**, 205 (2005).
[51] Z.-F. Cui, S.-S. Xu, B.-L. Li, A. Sun, J.-B. Zhang, and H.-S. Zong, Eur. Phys. J. C **78**, 770 (2018).
[52] S.-S. Xu, Z.-F. Cui, A. Sun, and H.-S. Zong, J. Phys. G **45**, 105001 (2018).
[53] C.-M. Li, P.-L. Yin, and H.-S. Zong, Phys. Rev. D **99**, 076006 (2019).
[54] L. Reinders, H. Rubinstein, and S. Yazaki, Phys. Rep. **127**, 1 (1985).
[55] T. G. Steele, Z. Phys. C **42**, 499 (1989).
[56] P. Pascual and R. Tarrach, *QCD: Renormalization for the Practitioner* (Springer, New York, 1984).
[57] P. Zyla, R. Barnett *et al.* (Particle Data Group) Prog. Theor. Exp. Phys. **2020**, 1 (2020).
[58] H.-S. Zong, L. Chang, F.-Y. Hou, W.-M. Sun, and Y.-X. Liu, Phys. Rev. C **71**, 015205 (2005).
[59] J.-L. Zhang, Y.-M. Shi, S.-S. Xu, and H.-S. Zong, Mod. Phys. Lett. A **31**, 1650086 (2016).
[60] H. Kohyama, D. Kimura, and T. Inagaki, Nucl. Phys. **B896**, 682 (2015).
[61] H.-S. Zong and W.-M. Sun, Int. J. Mod. Phys. A **23**, 3591 (2008).
[62] D. Lu, K. Tsushima, A. Thomas, A. Williams, and K. Saito, Nucl. Phys. **A634**, 443 (1998).
[63] G. Song, W. Enke, and L. Jiarong, Phys. Rev. D **46**, 3211 (1992).
[64] C.-M. Li, Y. Yan, J.-J. Geng, Y.-F. Huang, and H.-S. Zong, Phys. Rev. D **98**, 083013 (2018).
[65] Y. Yan, J. Cao, X.-L. Luo, W.-M. Sun, and H.-S. Zong, Phys. Rev. D **86**, 114028 (2012).
[66] O. G. Benvenuto and G. Lugones, Phys. Rev. D **51**, 1989 (1995).
[67] T. Hinderer, B. D. Lackey, R. N. Lang, and J. S. Read, Phys. Rev. D **81**, 123016 (2010).